Supplement of Ocean Sci., 22, 387–401, 2026
https://doi.org/10.5194/os-22-387-2026-supplement

Ocean Science Open Access EGU

Supplement of

Spatiotemporal scales of mode water transformation in the Sea of Oman

Estel Font et al.

Correspondence to: Estel Font (estel.font.felez@gu.se)

Content: Supplementary Text S1; Figures S1-S2:

- Section S1: Water Mass Transformation Framework
- Figure S1: Mode water definition: Potential vorticity (PV) vs. potential density criteria.
- Figure S2: Air-sea fluxes flag.

S1. Water Mass Transformation Framework

The following section describes a general method for representing changes in potential density (σ) and spice (τ) in the ocean as diapycnal and isopycnal (diaspice) transformations of water between water mass classes. The method used here to compute water-mass transformation in the sigma-spice (σ-τ) coordinates is based on the thermohaline derivation of Evans et al. (2014) and Portela et al. (2020) from the equations of tracer conservation:

$$\partial C/\partial t - \mathbf{u} \cdot \nabla C = k\nabla^2 C + f_c \qquad \text{(S1)}$$

where **u** is the three-dimensional Eulerian velocity, k is the diffusion coefficient, and f_C represents any source or sink of the given tracer C. Dividing the left-hand side of Eq. S1 by the modulus of the tracer gradient gives the dia-surface velocity component (u_C), the component of the velocity that crosses the surface of constant C. If we consider the tracers σ and τ, so that u_σ becomes the diapycnal velocity crossing the isopycnal σ and u_τ the dia-spice velocity crossing the iso-spice τ. Then, the transformation across sigma and spice surfaces can respectively be expressed as:

$$U_\sigma(\sigma,\tau) = \int_{\sigma'=\sigma} \Pi(\tau,\tau')\cdot u_\sigma \cdot dA \text{ and } \qquad U_\tau(\sigma,\tau) = \int_{\tau'=\tau} \Pi(\sigma,\sigma')\cdot u_\tau \cdot dA \qquad \text{(S2.1, S2.2)}$$

Where

$$\Pi(\sigma,\sigma') = \Pi(\tau,\tau') = \begin{cases} 1 \text{ if } \sigma \in \sigma' \text{ and } \tau \in \tau' \\ 0 \text{ otherwise.} \end{cases} \qquad \text{(S3)}$$

and $\sigma' = (\sigma \pm \Delta\sigma/2)$ and $\tau' = (\tau \pm \Delta\tau/2)$. Here, u_σ and u_τ are the diapycnal and isopycnal (diaspice) velocity components, respectively, and *dA* is the cross-sectional area of the transect occupied by water within the specified σ-τ class. These dia-surface transformations should be interpreted as volume fluxes of water and have units of $m^3\ s^{-1}$. They cannot be practically diagnosed from velocity measurements and must therefore be determined indirectly from changes in the volumetric distribution of water projected into *σ-τ* coordinates. In the case of a two-dimensional ocean transect, as per this study, the method is identical; however, the inferred transformations are area fluxes and have units of $m^2\ s^{-1}$.

We performed a volume budget in *σ-τ* coordinates for the interior ocean (i.e., below the mixed layer). The water-mass volume change *dV/dt* results from the sum of water-mass transformation, ∑U(σ,τ),

and the exchange flux across the domain's geographical limits Ψ (Evans et al., 2014; Portela et al., 2020). *U* is the water-mass transformation due to isopycnal and diapycnal mixing fluxes, whereas its convergence or divergence is represented by the sum (∑) of the interior fluxes across the geographical limits of a given *σ*-*τ* class (Donners et al. 2005; Walin 1982). The isopycnal and diapycnal transformation rates represent the net mixing of water masses along and across density surfaces, respectively, resulting in an irreversible property change. Ψ represents the net exchange across the northern boundary of the domain, defined as the northernmost bin of the glider and climatology transect. The southern end is shelf-constrained, and cross-section exchange there is assumed to be negligible. Note that an underestimation of the exchange flux Ψ could result in an apparent overestimation of the local transformation rate U. However, since both diapycnal and isopycnal transformations are estimated using the same underlying framework, there is no reason to expect a preferential bias toward either component. In summary, changes in volume within a given *σ*-*τ* class can be attributed to the convergence or divergence of interior fluxes across σ or τ boundaries, or via exchange fluxes across the domain boundaries within the same σ-τ class. Unlike interior mixing, exchange fluxes do not imply a transformation of water mass properties. The dia-surface transformations across each isopycnal and isospice are thus constrained by the volume changes of each *σ*-*τ* class. From expressions S1 and S2.1, S2.2; the volume change within a given *σ*-*τ* class can then be expressed as:

$$\frac{dV}{dt}(\sigma',\tau') = U_{\sigma}(\sigma',\tau') + U_{\tau}(\sigma',\tau') + \Psi(\sigma',\tau') \qquad \text{(S4)}.$$

The volume (area) changes are determined as follows. First, a nominal grid spacing in *σ*-*τ* coordinates is chosen. This grid spacing must be fine enough to resolve the finer water mass transformations in the specified region, but coarse enough to give adequate coverage in *σ*-*τ* coordinates so that there are not any artificially disconnected regions separated by no data. The volume integration was made in *σ*-*τ* classes with density intervals of $\Delta\sigma$=0.05 kg m^{-3} between 23 and 27.5 kg m^{-3} and spice intervals of $\Delta\tau$=0.1 kg m^{-3} between 4 and 8.5 kg m^{-3}. This choice reflects a trade-off between adequately representing each water mass class and ensuring that the mode water layer is well resolved. To calculate the water mass volume associated with each *σ*-*τ* class, the volume (area) of each geographical grid cell was calculated (i.e., along-transect x vertical extent for an ocean section). The *σ*-*τ* value at the center of each geographical grid cell was determined through linear interpolation. The volume for a given *σ*-*τ* class is then the sum of the volume associated with each geographical grid cell within the range σ ± Δσ/2 and τ ± Δτ/2.

Using Eq. S4, a set of linear equations can be built to link the observed change in volume of each *σ*-*τ* class, as determined above, to the dia-surface transformations:

$$\mathrm{d}\mathbf{V}/\mathrm{dt}=\mathbf{A}\mathbf{x} \qquad \text{(S5)}$$

Where:

- $\mathrm{d}\mathbf{V}/\mathrm{dt} = \left[\frac{dV}{dt}_{\sigma_1,\tau_1}, \frac{dV}{dt}_{\sigma_2,\tau_1}, \ldots, \frac{dV}{dt}_{\sigma_m,\tau_n}\right]$ and is a vector of the observed change in volume of each *σ*-*τ* class, divided by the relevant time interval, and should be m x n long, where m is the number of individual *σ* classes and n is the number of individual *τ* classes.

- The matrix **A** represents the coefficients relating each term on the right-hand side of Eq. S5 to the volume change. Each of the m x n rows represents the equation for the change in volume of a *σ*-*τ* class. The first [(m-1) x n]+[m x (n-1)] columns in **A** correspond to each *σ* or *τ*

iso-surface, and the coefficients describe the relation of each iso-surface to the σ-τ class designated in each row. A coefficient of 1 is assigned to the isopycnal (or isospice) at $\sigma - \Delta\sigma/2$; and a coefficient of -1 is assigned to the isopycnal (or isospice) at $\sigma + \Delta\sigma/2$. The coefficient is zero for each isopycnal and isospice that is not adjacent to the σ-τ class associated with the given row. The last m x n columns of **A** represent each σ-τ class, to which a coefficient of 1 is assigned if that value of σ or τ is adjacent to the boundary of the domain in geographical coordinates; thus allowing a flux into or out of the domain due to the terms combined into Ψ. Further, we are assuming that only advection through the northern boundary of the geographical domain will affect the distribution of volume.

- And the vector of unknowns **x** is the diapycnal and isopycnal (diaspice) transformations and the volume change associated with Ψ and it is defined as $\mathbf{x} = \left[U_{\sigma}^{1}, \ldots, U_{\sigma}^{m-1}, U_{\tau}^{1}, \ldots, U_{\tau}^{n-1}, \Psi^{1,1}, \ldots, \Psi^{m,n} \right]$. The length is [(m-1) x n]+[m x (n-1)] + (m x n).

The linear equation [5] can then be solved for **x** using a least squares regression, where the sum of the squared residuals ($(d\boldsymbol{V}/dt) - \mathbf{A}\mathbf{x}$) are minimized. The residual errors for both datasets, computed as $|(d\boldsymbol{V}/dt) - \mathbf{A}\mathbf{x}|/|(d\boldsymbol{V}/dt)|$, were on average of order 10^{-5}, which is on the higher end of values reported in previous studies (e.g., Portela et al., 2020). The derived transformations, therefore, represent the minimum combination of volume fluxes required to explain the volume change of each σ-τ class. To note, because the exchange term Ψ is obtained as part of the least-squares solution to Eq. S5 rather than by a simple difference of diagnosed terms, it is constrained jointly with U_{σ} and U_{τ}. We therefore interpret Ψ as an effective advective exchange term. The solution **x** was then decomposed into the transformation across spice and density surfaces and the exchange flux across the geographical domain. See also Evans et al (2014) and Portela et al (2020) for other explanations of the methodology.

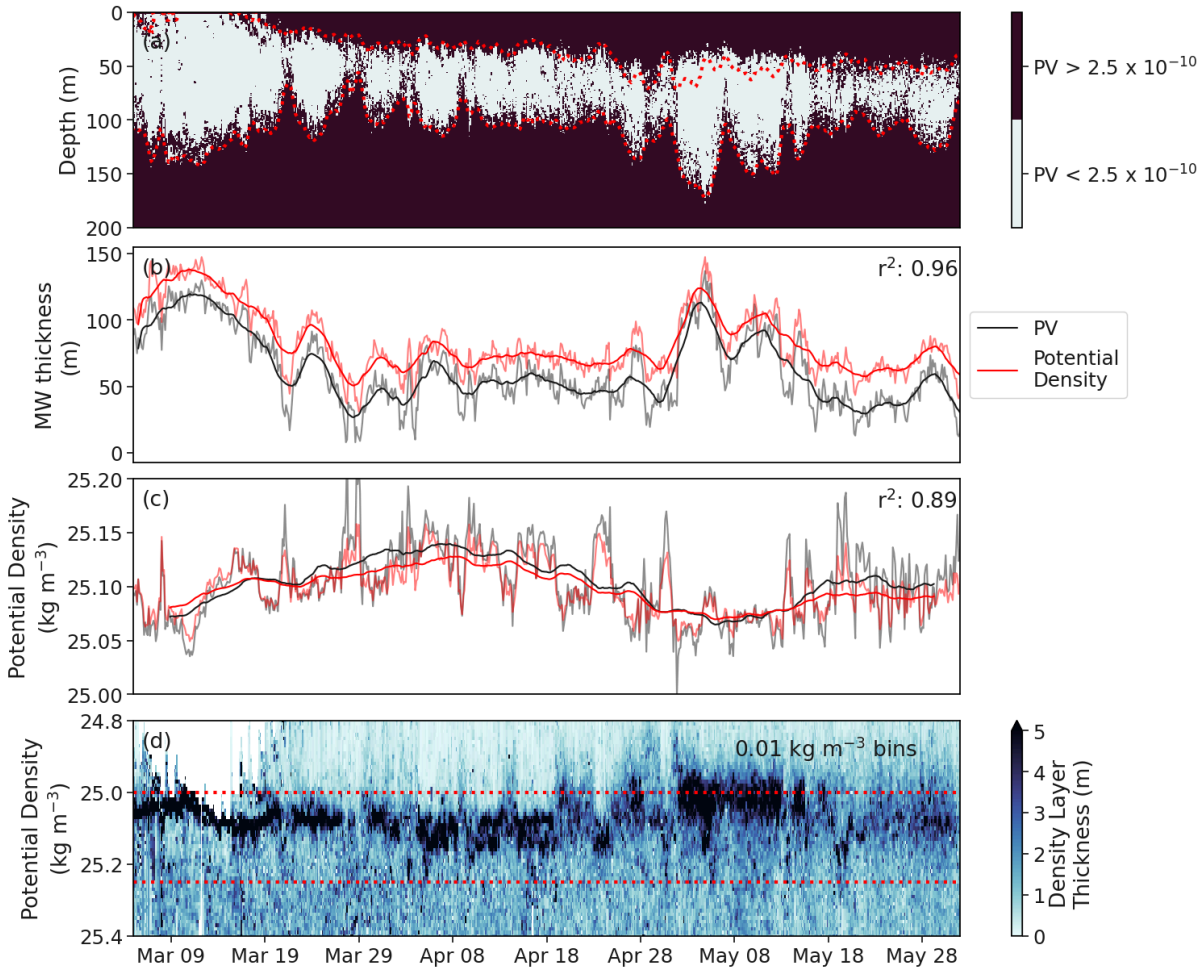

Figure S1. Mode water definition: Potential vorticity (PV) vs. potential density criteria. *a) Ocean glider timeseries colored by PV smaller or larger than the median PV (2.5 x 10^{-10} s-2). Red contours are the 25 and 25.25 kg m^{-3} isopycnals. b) Mode water thickness using the PV criteria (black) and density criteria (red) for the original time series and 24 h rolling mean. The coefficient of determination (r^2) is 0.96 between these two methods. c) Mode water density using the PV criteria (black) and density criteria (red) for the original time series and 24 h rolling mean. The r^2 is 0.89 between these two methods. d) Potential density layer thickness per 0.01 kg m^{-3} bins in potential density space. Red lines are the 25 and 25.25 kg m^{-3} isopycnals.*

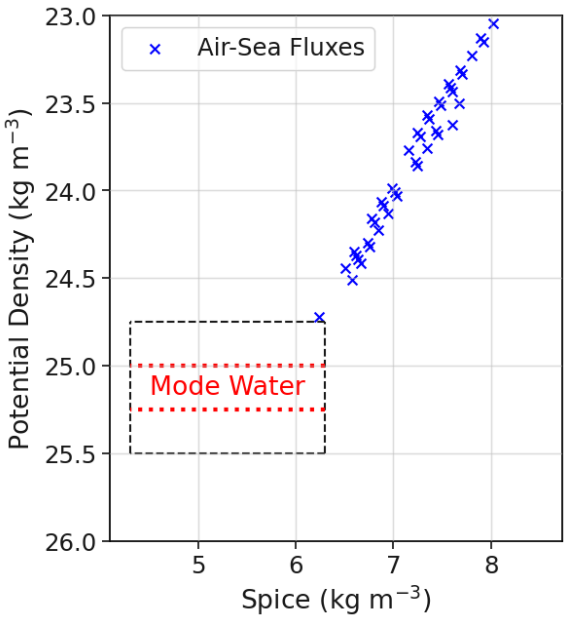

Figure S2: Air-sea fluxes flag. *The volume of water bound by a given tracer surface will change by air–sea buoyancy fluxes if the tracer surface outcrops at the ocean surface. We compute the transformation in T-S coordinates as per Evans et al. (2014, 2023) and retrieve the classes that change due to air-sea buoyancy fluxes. The T-S classes are afterwards converted to σ-τ space and are marked as blue crosses. The box shows the σ-τ domain of interest for this study, and the red lines show the mode water potential density band, which lies below the classes affected by the air-sea interface. Air-sea buoyancy fluxes used were derived from the ERA5 reanalysis product (Hersbach et al., 2020), matched to the glider's position and time for high-resolution analysis, and also retrieved as monthly climatological averages over the study area.*

References

Donners, J., Drijfhout, S. S., and Hazeleger, W.: Water mass transformation and subduction in the South Atlantic, J. Phys. Oceanogr., 35, 1841–1860, https://doi.org/10.1175/JPO2782.1, 2005.

Evans, D. G., Zika, J. D., Naveira Garabato, A. C., and Nurser, A. J. G.: The imprint of Southern Ocean overturning on seasonal water mass variability in Drake Passage, J. Geophys. Res.-Oceans, 119, 7987–8010, https://doi.org/10.1002/2014JC010097, 2014.

Evans, D. G., Holliday, N. P., Bacon, S., and Le Bras, I.: Mixing and air–sea buoyancy fluxes set the time-mean overturning circulation in the subpolar North Atlantic and Nordic Seas, Ocean Sci., 19, 745–768, https://doi.org/10.5194/os-19-745-2023, 2023.

Hersbach, H., Bell, B., Berrisford, P., Hirahara, S., Horányi, A., Muñoz-Sabater, J., Nicolas, J., Peubey, C., Radu, R., Schepers, D., Simmons, A., Soci, C., Abdalla, S., Abellan, X., Balsamo, G., Bechtold, P., Biavati, G., Bidlot, J., Bonavita, M., De Chiara, G., Dahlgren, P., Dee, D., Diamantakis, M., Dragani, R., Flemming, J., Forbes, R., Fuentes, M., Geer, A., Haimberger, L., Healy, S., Hogan, R. J., Hólm, E., Janisková, M., Keeley, S., Laloyaux, P., Lopez, P., Lupu, C., Radnoti, G., de Rosnay, P., Rozum, I., Vamborg, F., Villaume, S., and Thépaut, J. N.: The ERA5 global reanalysis, Q. J. Roy. Meteor. Soc., 146, 1999–2049, https://doi.org/10.1002/qj.3803, 2020.

Portela, E., Kolodziejczyk, N., Maes, C., and Thierry, V.: Interior water-mass variability in the Southern Hemisphere oceans during the last decade, J. Phys. Oceanogr., 50, 361–381, https://doi.org/10.1175/JPO-D-19-0128.1, 2020.

Walin, G.: On the relation between sea-surface heat flow and thermal circulation in the ocean, Tellus, 34, 187–195, https://doi.org/10.3402/tellusa.v34i2.10801, 1982.